

Prototype of pneumo-electromagnetic drive operating in motor and generator modes for compressed air energy storage systems

Jacek Leszczyński^{1*}, Dominik Gryboś², Bartosz Kozera²

¹AGH University of Science and Technology, Faculty of Energy and Fuels, Department of Thermal and Fluid Flow Machines, Cracow, Poland
(Corresponding Author)

²AGH University of Science and Technology, Faculty of Energy and Fuels, Department of Thermal and Fluid Flow Machines, Cracow, Poland

ABSTRACT

This paper presents a prototype of a pneumo-electromagnetic drive operating in reverse mode. Preliminary test results are presented. An example design is shown.

Keywords: renewable energy resources, CAES, linear engine/generator, reverse operation, magnetic flux, low pressure

NOMENCLATURE

<i>Abbreviations</i>		φ	relative air humidity, –
CAES	compressed air energy system		
PMSG	permanent magnet synchronous generator		
<i>Uppercase letter</i>		<i>Subscripts</i>	
A	cross-section, m ²	0	ambient, initial
D	diameter, m	1+X	moist air
E	energy, kJ	A,B	pointers
F	force, N	a	air
N	number, -	b	begin
I	current, A	e	end
L	inductance, H	g	gauge
P	power, W	G	gravity
	individual gas constant, $\frac{J}{kgK}$, resistance,		
R	Ω	i	index, pointer, i=...0,1,2
T	temperature, K	max	maximum
U	voltage, V	min	minimum
V	volume, m ³	pb	pole pairs
V	volume flow, $\frac{m^3}{s}$	pr	piston rod
X	humidity ratio, –	s	saturation
<i>Lowercase letter</i>		T	transmission
d	diameter, m	x	additional
l	length, m	LG	linear generator
m	mass, kg	TB	transmission air
\dot{m}	mass flow, $\frac{kg}{s}$		
p	pressure, Pa		
s	stroke, m		
t	time, s		
v	piston velocity, $\frac{m}{s}$		

w	piston thickness, m		
<i>Greek symbols</i>		<i>Constants</i>	
β	critical pressure ratio, –	$\kappa = 1.4$	adiabatic exponent for air, –
Δ	interval, –	$g = 9.81$	acceleration due to gravity force, $\frac{m^2}{s}$
ϵ	electromotive force, V	$P_0 = 101235$	ambient pressure, Pa
η	efficiency, –	$R_a = 287.1$	individual gas constant air, $\frac{J}{kgK}$
κ	adiabatic exponent, –	$R_w = 461.4$	individual gas constant water vapour, $\frac{J}{kgK}$
ζ	scaling factor, –		
v	specific volume, $\frac{m^3}{kg}$		
ρ	density, $\frac{kg}{m^3}$		
Φ	magnetic flux, Wb		

1. INTRODUCTION

Compressed air energy system technology is well-known and continuously used in the power industry, e.g. in Huntorf, Germany, where it has been exploited for over 40 years. [1] The basis of compressed air energy storage systems is to utilise the extra energy from the grid that compressors would waste. The compressed air is stored in tanks or caverns and then released to turbines connected to generators at times of high grid demand. [14,15] It can also store a large amount of energy. The idea of utilising this kind of storage installation has many advantages. The main disadvantage of the classic CAES system is the need to burn fossil fuels – it needs to be coupled with a gas turbine plant. [16] With energy storage being such an important issue, many researchers are trying to examine other types of CAES that do not need fossil fuels, for example, coupled with heliostat solar fields [17], biomass [18], wind farms [19] or geothermal energy [21]. There are several papers with proposals for utilising compressed air, e.g. in bus engines [20] or motor engines [22]. Still, few papers show how to use this type of energy in low-pressure ranges. The most common type of energy generation in CAES is shaft-connected turbines with a generator. The gas expander inlet pressure in this type of system is approximately 20 bar, according to Salvini C. [2]. Also, for already existing CAES power plants, the operating pressure on the turbines is set at 41 - 42 bar for both Huntorf and McIntosh systems. [3,13] When the pressure is not that high, and the compressed air volume is low, turbine generation technology is not well suited. In this case, we propose a prototype linear generator.

This is where the linear pneumo-electromagnetic drive comes in. Low investment costs, simple construction, long service life, compact size, the

possibility of reverse mode, and working as a generator and motor speak for the utility of this type of technology in low-pressure systems. The main advantage is the omission of a timing gear system.

The traditional linear alternator is constructed in a cylindrical or flat shape. The most common way is tubular technology. In paper [4], a hybrid design with a flat and cylindrical shape was developed. Moving a piston with a magnet using compressed air generates electrical energy on the cylinder side coils. The main disadvantage of the proposed construction is the complex design with valves as in a classic engine. This can cause many maintenance problems. The highest efficiency of the generator was obtained at 4 bar and 93.6 %. The conversion efficiency at the same air parameters was over 45 %.

In other papers, a low-pressure linear generator was presented by Peng B. [5]. The proposed system operates in the pressure range of 3 - 7 bar achieving more than 3 % generation efficiency with a 24 V maximum voltage and a maximum current of 2.5 A.

The work of Guo Ch. [6] presents a prototype of a linear generator with a combustion chamber. The operation principle is common to the compressed air device - the fuel combustion process forces the piston movement. The efficiency of the proposed system is estimated at 36.2 % and 42 %, depending on the combustion mode. The main disadvantage of the system is the exhaust gas, which can be eliminated by using compressed air.

In this paper, we would like to introduce a linear generator which is driven by compressed air. The construction comprises two steel plates with permanent magnets and six coils laminated with epidian resin, which are connected to a pneumatic actuator. The coils move in both directions generating electricity. The innovation of this Prototype lies mainly in the simplicity of the

design. It is also possible to reverse the operation of the Prototype by delivering current to the coils. In this case, the air is compressed by the piston of the pneumatic drive, which is moved by electromagnetic forces caused

by the supplied energy. The compressed air is stored in unique pressure-proof tanks and can be used to power the generator in case of high energy demand.

2. EXPERIMENTAL SETUP AND THEORETICAL BACKGROUND

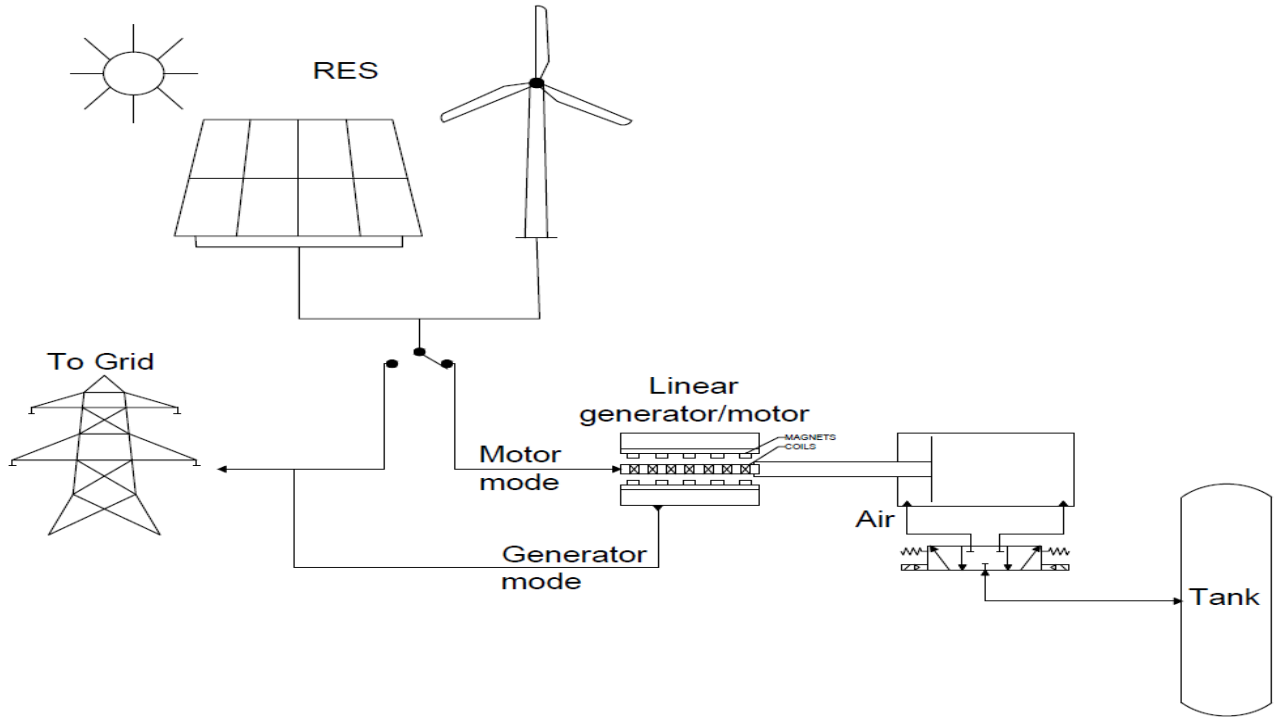


Fig. 1 Proposal for the use of the Prototype in an advanced system.

2.1 Experimental setup

The experimental setup contains the generator/motor unit described in this paper, pneumatic drive, compressed air tank, and renewable energy sources (Fig.1). The prototype core concept is shown in Fig.1. It is made of two construction shields made of steel (S235) to prevent the magnetic flux from escaping the structure. There are 6 magnets on both of the shields to generate magnetic flux. In the centre of construction, there are coils coupled to a pneumatic drive which move in a reciprocating motion.

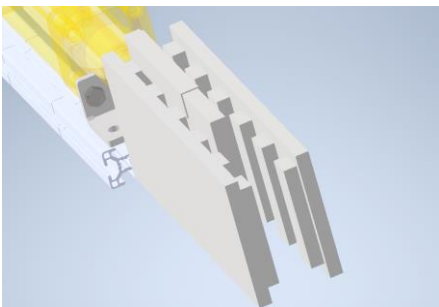


Fig.2 Theoretical construction of Prototype - core.

The coil core (2) made of epidian resin is shown in Fig.3 and Fig.4. The core contains 6 copper coils which are divided into 3 current phases and is driven by a piston rod (3) in reciprocating movement. The Prototype is covered with magnetic screens (1), forcing magnetic flux to stay inside the construction. Linear runners were fitted at the bottom and top to protect the core from bending forces and deflection from the prototype axis. The pneumatic drive was centred on forcing movement on the axis between the 2 steel magnetic plates. The whole system is powered by a compressor with a range of 1.4-6 bar, which is connected by a three-way valve to the pneumatic drive (3). The moment of core direction change is affected by reed sensors connected to the PLC unit (5) shown in Fig.5, which also controls the three-way valve (7) to deliver compressed air at the appropriate moment. To measure the DC current, the coils are connected to a rectifier diode bridge.

The design incorporates 12 magnets on steel plates that act as magnetic screens and 6 coils made of 32 copper coils each. The wire diameter is estimated to be

1.3 mm. Magnetic screens are made of S235 steel – 200x300x15 mm each.

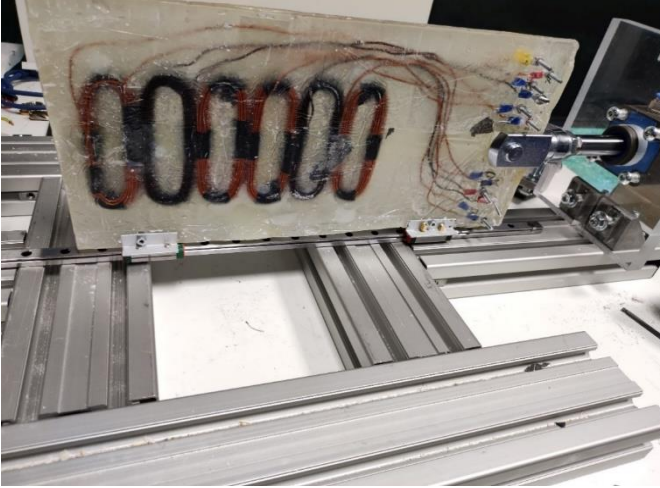


Fig.3 Construction of Prototype - core.

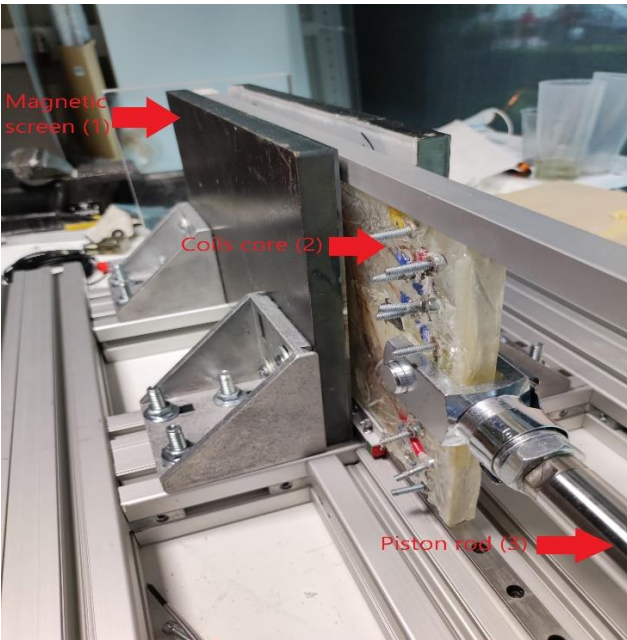


Fig.4 Construction of Prototype – core with magnet plates.

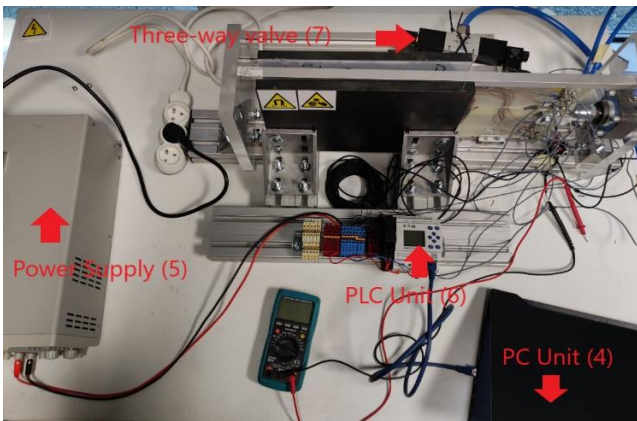


Fig.5 Construction of Prototype – measuring system.

2.2 Theoretical background

The mathematical model of piston rod movement is described by equations shown below according to our previous studies [9].

$$\left\{ \begin{array}{l} \frac{dm_2}{dt} = \dot{m}_1 + \dot{m}_3 \\ \frac{dm_4}{dt} = \dot{m}_4 \\ \frac{dm_5}{dt} = \dot{m}_5 \\ m \frac{d^2y}{dt^2} = F_4 + F_5 + F_v + F_g + F_e \\ L \frac{dI}{dt} = \frac{dy}{dt} Bl - I(R_g - R_{LOAD}) \end{array} \right. \quad (1)$$

where: mass of moist air in the storage tank m_2 , mass of moist air under a piston m_4 , mass of moist air over a piston and m_5 , mass flow entering the storage tank \dot{m}_1 , mass flow exiting a tank \dot{m}_3 , mass flow entering or exiting under a piston \dot{m}_4 , mass flow entering or exiting over a piston \dot{m}_5 , mass of the mechanical elements m , piston position y , time t , driving/braking force under a piston F_4 , driving/braking force over a piston F_5 , friction force F_v which contains Coulomb and viscous friction [10], gravitational force F_g , electromagnetic force F_e stator winding resistance of LG R_g , stator winding inductance of LG L , load resistance R_{LOAD} , voltage U , current I .

The driving/braking force under the piston F_4 ,

$$F_4 = A_4 p_4 \quad (2)$$

and driving/braking force above the piston F_5 ,

$$F_5 = -(A_4 - A_5) p_5 \quad (3)$$

The geometrical quantities are as follows:

-piston stroke

$$s = y_e - y_b \quad (4)$$

where: beginning, ending position of the piston y_b, y_e respectively

– surface areas of elements A_i and pipes a_i ,

$$A_i = \frac{\pi D_i^2}{4} \quad (5)$$

for $i = 2,4,5$

$$a_i = \frac{\pi d_i^2}{4} \quad (6)$$

for $i = 1, \dots, 5$

– harmful volumes existing in a cylinder under or above the piston $V_{0;4}, V_{0;5}$

$$V_{0;4} = A_4 l_{0;4} \quad (7)$$

$$V_{0;5} = (A_4 - A_5) l_{0;5} \quad (8)$$

where: initial lengths $l_{0;4}, l_{0;5}$.

– cylinder volumes – variable volumes in a cylinder existing under and above the piston V_4, V_5

$$V_4 = A_4(y - y_b) + V_{0;4} \quad (9)$$

$$V_5 = (A_4 - A_5)(y - y_b - w l_2) + V_{0;5} \quad (10)$$

where: piston thickness w .

- storage tank volumes V_2 ,

$$V_2 = l_2 A_2 \quad (11)$$

where: tank height/length l_2 .

Physical quantities are as follows:

– overall mass in motion m ,

$$m = m_p + m_{pr} + m_6 + m_x \quad (12)$$

where: mass of the piston m_p , mass of the piston rod m_{pr} , rack mass m_6 , additional mass m_x .

- absolute pressures p_i ,

$$p_i = p_0 + p_{g;i} \quad (13)$$

for $i = 1,2,7,8$, where: indicate gauge pressures $p_{g;i}$, ambient pressure p_0 .

Auxiliary functions are as follows:

– water vapour saturation pressure p_s ,

$$p_s = 611.2 e^{\frac{17.62(T-273)}{243.12+(T-273)}} \quad (14)$$

- humidity ratio X

$$X = \frac{R_a}{R_w} \frac{\phi \frac{p}{p_0} p_s(T)}{p - \phi \frac{p}{p_0} p_s(T)} \quad (15)$$

– individual gas constant mixture of gas with water vapour R_{1+X}

$$R_{1+X} = R_w \frac{\frac{R_a}{R_w} + X}{1 + X} \quad (16)$$

– specific volume of moist air v_{1+X} ,

$$v_{1+X} = R_w \left(\frac{R_a}{R_w} + X \right) \frac{T}{p} \quad (17)$$

– density of moist air ρ_{1+X} ,

$$\rho_{1+X} = \frac{1 + X}{v_{1+X}} \quad (18)$$

– mass of moist air in the tank m ,

$$m = \frac{\left(1 - \left(1 - \frac{R_a}{R_w}\right) \phi \frac{p_s(T)}{p_0}\right) p V}{R_a T} \quad (19)$$

- absolute pressure p ,

$$m = \frac{R_a T m_a}{\left(1 - \left(1 - \frac{R_a}{R_w}\right) \phi \frac{p_s(T)}{p_0}\right) V} \quad (20)$$

where: air mass m_a , critical pressure ratio β , air density ρ , adiabatic exponent κ , area A , pressure p , temperature T , air constant R_a , vapour constant R_w , saturation pressure p_s , pressure p_0 , volume V .

The well-known 1-d steady fluid dynamics equations [11] were used to describe mass flow between system parts, as shown below.

$$\dot{m} = \begin{cases} A \sqrt{\frac{2\kappa}{\kappa-1} \rho p_A \left(\frac{p_B}{Z p_A}\right)^{\frac{2}{\kappa}} - \left(\frac{p_B}{Z p_A}\right)^{\frac{\kappa+1}{\kappa}}} & \text{for } \frac{p_B}{p_A} > \beta \\ A \sqrt{\rho p_A \left(\frac{2}{\kappa+1}\right)^{\frac{\kappa+1}{\kappa-1}}} & \text{for } \frac{p_B}{p_A} < \beta \end{cases} \quad (21)$$

where: critical pressure ratio β ,

$$\beta = \zeta \left(\frac{2}{\kappa + 1} \right)^{\frac{\kappa}{\kappa - 1}} \quad (22)$$

A slight modification was noted in Eq. (24) and Eq. (25). Here we introduce a scaling function Z,

$$Z = \frac{1 - \zeta}{1 - \beta^{2\zeta}} \left(\frac{p_A}{p_B} \right)^{2\zeta} + \frac{\zeta - \beta^{2\zeta}}{1 - \beta^{2\zeta}} \quad (23)$$

which involves the numerical factor ζ . Such a factor type takes values from 0 to 1. In classical thermodynamics [11], critical pressure ratio equals $\beta = 0.53$. However, as noted in [12], there are plenty of cases when the critical pressure ratio is $\beta < 0.53$. It means that the choked flow

range finishes faster, and the subsonic flow operates in the higher pressure ratio range. This happens when the transition connecting the cross-sections is sharp-edged. According to thermodynamics [11], we noticed a contraction of the cross-section and therefore, the flow is choked.

-electrical power equation,

$$P_{LG} = UI \quad (24)$$

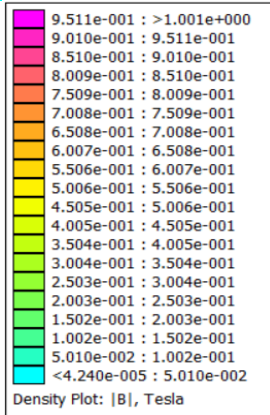
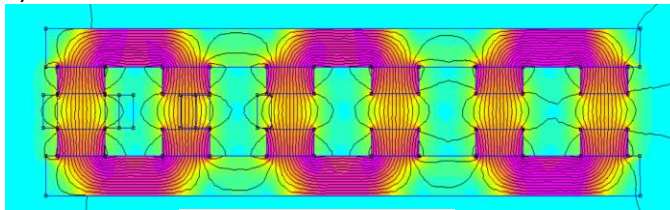
-the efficiency of converting the second transmission air power P_{TB} to the maximum electrical power generated by linear generator unit P_{LG} ,

$$\eta_{LG} = \frac{P_{LG}}{P_{TB}} \quad (25)$$

3. RESULTS

The study included magnetic flux analysis and electrical power estimation. The proposed linear generator is estimated to work with maximum pressure $p_A = 6$ [bar]. The radius of the piston rod is $d = 50$ mm. Piston velocity is estimated at 0.5 - 2 m/s level. The Prototype is being constructed for 6 V. Fig. 6 shows magnetic density flux in the construction and in the axis of the Prototype. The maximum value in magnetic screens is estimated to be 0.95 T, when in axis 0.63 T.

a)



b)

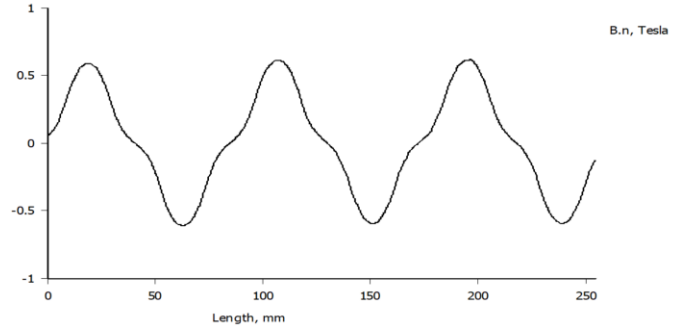


Fig. 6 Experimental data: a) Magnetic density flux in construction b) Normal magnetic density in axis of Prototype.

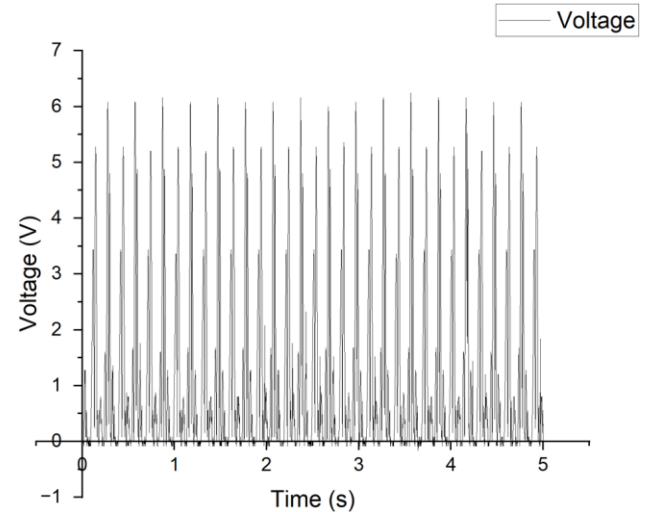


Fig. 7 Voltage during experiment with 6 bar pressure of compressed air – idle.

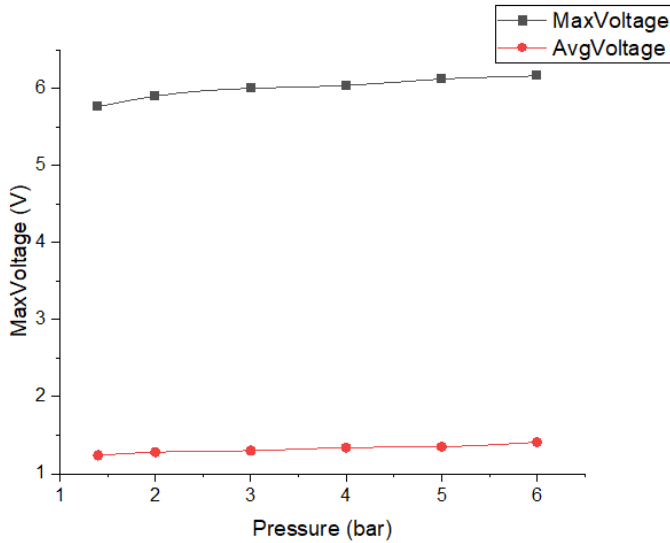


Fig. 8 Average and max voltage for idle working mode.

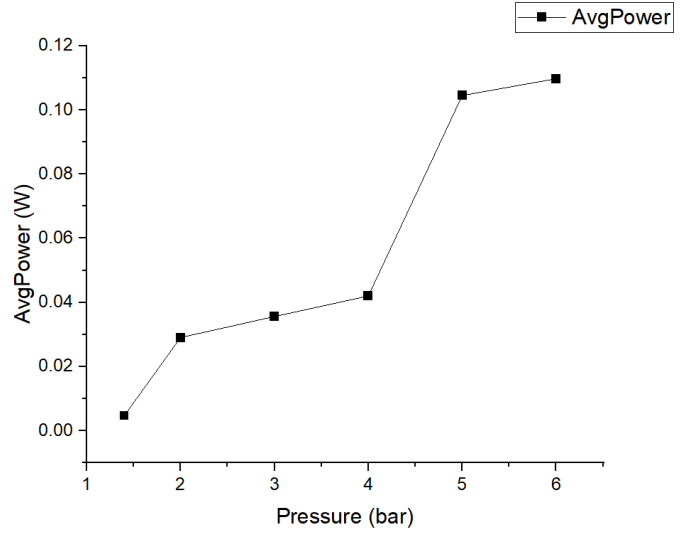


Fig. 11 Average power obtained in Prototype with 0.45 Ω load.

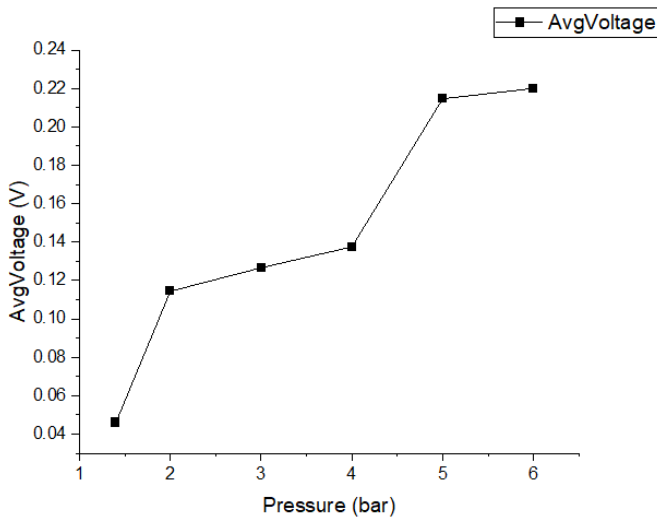


Fig. 9 Average voltage obtained in Prototype with 0.45 Ω load.

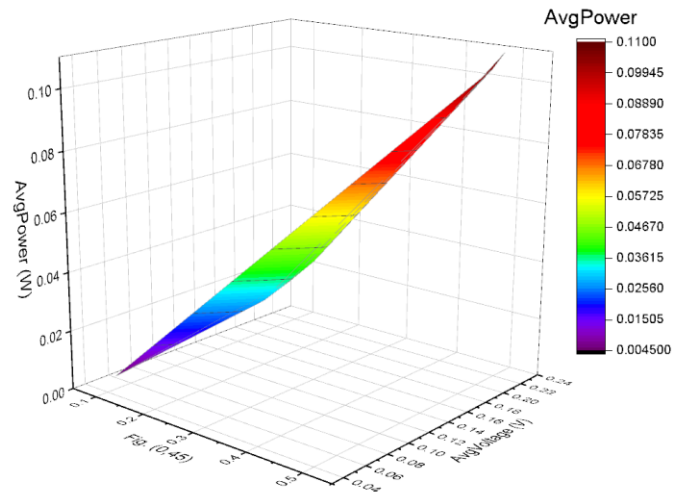


Fig. 12 Average power obtained in Prototype with 0.45 Ω load related to current and voltage.

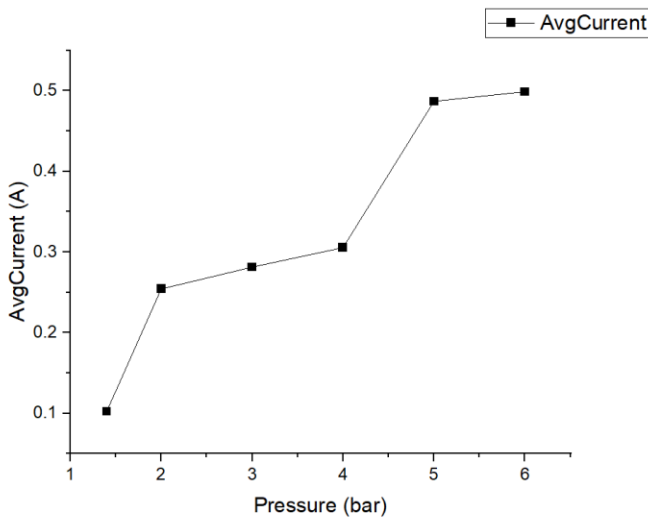


Fig. 10 Average current obtained in Prototype with 0.45 Ω load.

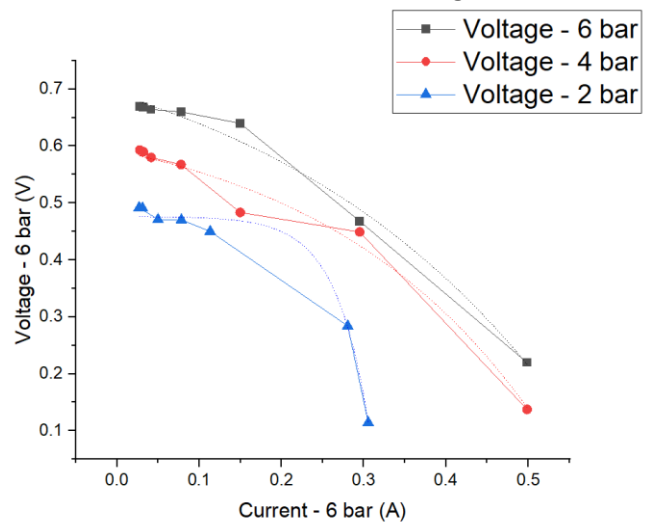


Fig. 13 Current-voltage characteristics for variable pressure.

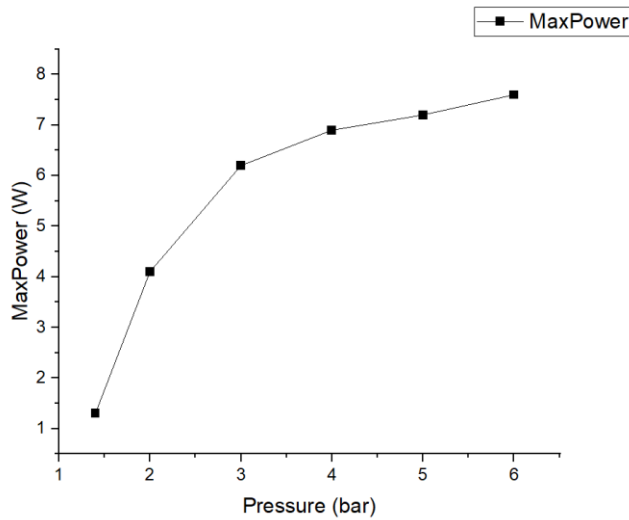


Fig. 14 Maximum power obtained in construction.

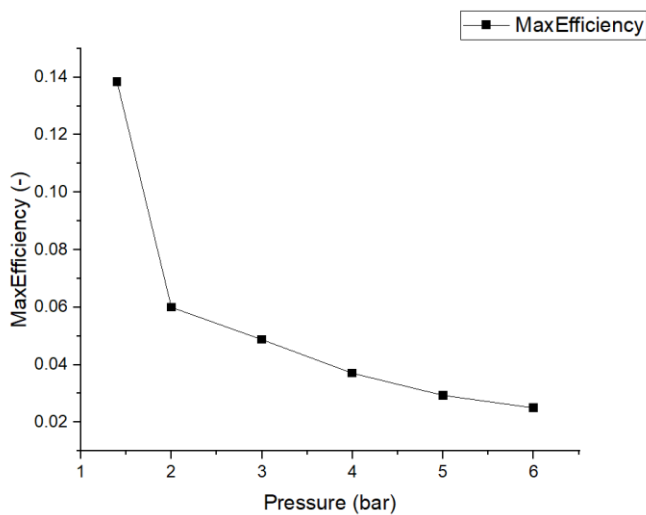


Fig. 14 Maximum efficiency in Prototype.

As shown in Fig.7 obtained voltage for the small Prototype proposed in this work is estimated at a maximum level of 6 V. It can be observed that when increasing the pressure from the tank to the construction, the achieved voltage is slightly higher. Due to the low average voltage level, it is recommended in future prototypes to increase the length of the magnetic screens and the number of magnets and coils, which would increase the power. Due to too many changes in the direction of movement of the coil core, the time during which the linear generator does not produce any electromotive force is too long. This results in a low average power level in the system. Extending the piston rod, magnetic screens, and core would give much better results.

The obtained power level for a 0.45 Ω load was determined to be 0.11 W peak, with 0.52 V voltage and 0.22 A current, respectively. It can be observed that the device operates approximately 10x more efficiently at 6 bar than at 1.5 bar. While analysing Fig.13, it can be

observed that the maximum power obtained in Prototype is about 7-8 W, but coupled with Fig.14; it can be observed that maximum efficiency appears for the lowest pressure level of the tank – 14 %, respectively. This shows how the Prototype can be improved in the future because the proposed generator is too small for the proposed high energy source and does not utilise the maximum level of energy delivered. A much longer piston rod with a larger coil core can also be moved with similar parameters to the energy source mentioned – compressed air at a pressure of about 6 bar. It would affect with efficiency increase and what is also essential – power increase.

In summary, the performance of the Prototype could be significantly higher when the device is enlarged.

4. CONCLUSIONS

The Prototype is an exciting idea for compressed air energy utilisation – thanks to the simplicity of construction and high resilience. Optimisation of the proposed device could result in a considerable increase in efficiency and power delivered to the grid. The main conclusion from the work could be that device is unlikely to be the best solution for small-scale systems – such as smart home systems with microCAES (due to need for device enlargement). Still, it could give excellent results for larger systems where small-scale generators are not needed.

ACKNOWLEDGEMENT

The work was carried out as part of a research subvention under contact no. 16.16.210.476 awarded by the Polish Ministry of Science and Higher Education.

REFERENCE

- [1] Crotagino F., Mohmeyer K., Scharf R., Huntorf CAES: More than 20 Years of Successful Operation; 2021
- [2] Salvini C., Giovannelli A., Techno-economic comparison of diabatic CAES with artificial air reservoir and battery energy storage systems, Energy Reports; 2022, 8, 601-607.
- [3] Budt M., Wolf D., Span R., Yan J. A review of compressed air energy storage: Basic principles, past milestones and recent developments. Applied Energy; 2016, 170, 250-268.
- [4] Yongming X., Xiangfeng X., Yaodong W. Mengmeng A. Performance characteristics of compressed air-driven free-piston linear generator (FPLG) system – A simulation study. Applied Thermal Engineering; 2019,160,114013.
- [5] Peng B., Tong L., Yan D., Huo W. Experimental research and artificial neural network prediction of free piston expander-linear generator. Energy Reports;2022, 8, 1966-1978.

- [6] Guo Ch., Zuo Z., Feng H., Jia B., Roskilly T. Review of recent advances of free-piston internal combustion engine linear generator. *Applied Energy*;2020,269, 115084.
- [7] Meeker D. FEMM - Finite Element Method Magnetics Version 4.2 User's Manual.; October 2015.
- [8] Leszczyński J., Gryboś D., Kozera B., Pending patent Method of compressed air energy conversion by low pressure, linear energy converter.; 2022.
- [9] Leszczyński J., Gryboś D. Sensitivity analysis of Double Transmission Double Expansion (DTDE) systems for assessment of the environmental impact of recovering energy waste in exhaust air from compressed air systems. *Applied Energy*;2020, 278, 115696.
- [10] Armstrong-Helovry B. Control of machines with friction. 1st ed London: Kluwer Academic Publishers.; 1991.
- [11] Cengel YA, Boles MA. Thermodynamics. An engineering approach. 8th ed.; Mc. Graw–Hill Education; 2015.
- [12] Yang F, Li G, Hu D, Kagawa T. A new method for calculating the sonic conductance of airflow through a short tube. *Adv Mech Eng* 2016;9:1–13.
- [13] Arsie I., Marano V., Rizzo G., Optimal management of Wind/CAES Power Plant by Means of Neutral Network Wind Speed Forecast. *European Wind Energy Conference*;2007.
- [14] Milewski J., Badyda K., Szablowski Ł. Compressed Air Energy Storage Systems, *Journal of Power Technologies*;2016, 96,245-260.
- [15] H. Chen, T. Ngoc, W. Yang, C. Tan, Y. Li, Progress in electrical energy storage system : a critical review, *Prog. Nat. Sci*; 2009,19,291–312.
- [16] Denholm P, Kulcinski GL. Life cycle energy requirements and greenhouse gas emissions from large scale energy storage systems. *Energy Convers Manage* 2004;45:2153–72.
- [17] Kandezi MS., Naeenian SMM. Thermodynamic and economic analysis of a novel combination of the heliostat solar field with compressed air energy storage (CAES); a case study at San Francisco, USA. *Journal of Energy Storage*; 2022, 49, 104111.
- [18] Lashgari F., Babei SM., Pedram MZ., Arabkoohshar A. Comprehensive analysis of a novel integration of a biomass-driven combined heat and power plant with a compressed air energy storage (CAES). *Energy Conversion and Management*; 2022, 255, 115333.
- [19] Razmi AR., Soltani M., Ardehali A., Gharali K. Dusseault MB., Nathwani J. Design, thermodynamic, and wind assessments of a compressed air energy storage (CAES) integrated with two adjacent wind farms: A case study at Abhar and Kahak sites, Iran. *Energy*; 2021, 221, 119902.
- [20] Wang L., Zhu SL., Zhang XR., Zhang Hy. Another way of cleaner public transportation: Four-stroke high torque CAE (Compressed Air Engine) performance analysis and CAE bus. *Energy Reports*; 2022, 8, 5727-5738.
- [21] Mousavi SB., Ahmadi P., Pourahmadiyan A., Hanafizadech P. A comprehensive techno-economic assessment of a novel compressed air energy storage (CAES) integrated with geothermal and solar energy, *Sustainable Energy Technologies and Assessments*; 2021, 47, 101418.
- [22] Wang YW., You JJ., Sung CK., Huang CY. The Applications of Piston Type Compressed Air Engines on Motor Vehicles. *Procedia Engineering*; 2014, 79, 61-65.